Redox Biology 14 (2018) 164–177

Contents lists available at ScienceDirect

Redox Biology

journal homepage: www.elsevier.com/locate/redox

Research Paper

The 2-oxoglutarate carrier promotes liver cancer by sustaining mitochondrial GSH despite cholesterol loading

Anna Baulies[a,b,1], Joan Montero[a,b,2,3], Nuria Matías[a,b,3], Naroa Insausti[a,b], Oihana Terrones[c], Gorka Basañez[c], Carmen Vallejo[a,b], Laura Conde de La Rosa[a,b], Laura Martinez[a,b], David Robles[a,b], Albert Morales[a], Joaquin Abian[d], Montserrat Carrascal[d], Keigo Machida[e], Dinesh B.U. Kumar[e], Hidekazu Tsukamoto[e,f], Neil Kaplowitz[g], Carmen Garcia-Ruiz[a,b,e,g,*], José C. Fernández-Checa[a,b,e,g,*]

[a] Department of Cell Death and Proliferation, Instituto de Investigaciones Biomédicas de Barcelona, Consejo Superior de Investigaciones Científicas, 08036 Barcelona, Spain
[b] Liver Unit and Hospital Clínic i Provincial, IDIBAPS, and Centro de Investigación Biomédica en Red (CIBERehd), Spain
[c] Unidad de Biofísica (Centro Mixto Consejo Superior de Investigaciones Científicas-Universidad del País Vasco/Euskal Herriko Unibertsitatea), Universidad del País Vasco/Euskal Herriko Unibertsitatea, 48080 Bilbao, Spain
[d] CSIC/UAB Proteomics Laboratory, IIBB-CSIC, 08036 Barcelona, Spain
[e] Southern California Research Center for ALPD and Cirrhosis, Los Angeles, CA, USA
[f] Department of Veterans Affairs Greater Los Angeles Healthcare System, Los Angeles, CA, USA
[g] University of Southern California Research Center for Liver Diseases, Keck School of Medicine, USC, Los Angeles, CA, USA

ARTICLE INFO

Keywords:
Cholesterol
Hepatocellular carcinoma
Mitochondria
Small solute carriers
Hypoxia

ABSTRACT

Cancer cells exhibit mitochondrial cholesterol (mt-cholesterol) accumulation, which contributes to cell death resistance by antagonizing mitochondrial outer membrane (MOM) permeabilization. Hepatocellular mt-cholesterol loading, however, promotes steatohepatitis, an advanced stage of chronic liver disease that precedes hepatocellular carcinoma (HCC), by depleting mitochondrial GSH (mGSH) due to a cholesterol-mediated impairment in mGSH transport. Whether and how HCC cells overcome the restriction of mGSH transport imposed by mt-cholesterol loading to support mGSH uptake remains unknown. Although the transport of mGSH is not fully understood, SLC25A10 (dicarboxylate carrier, DIC) and SLC25A11 (2-oxoglutarate carrier, OGC) have been involved in mGSH transport, and therefore we examined their expression and role in HCC. Unexpectedly, HCC cells and liver explants from patients with HCC exhibit divergent expression of these mitochondrial carriers, with selective OGC upregulation, which contributes to mGSH maintenance. OGC but not DIC downregulation by siRNA depleted mGSH levels and sensitized HCC cells to hypoxia-induced ROS generation and cell death as well as impaired cell growth in three-dimensional multicellular HCC spheroids, effects that were reversible upon mGSH replenishment by GSH ethyl ester, a membrane permeable GSH precursor. We also show that OGC regulates mitochondrial respiration and glycolysis. Moreover, OGC silencing promoted hypoxia-induced cardiolipin peroxidation, which reversed the inhibition of cholesterol on the permeabilization of MOM-like liposomes induced by Bax or Bak. Genetic OGC knockdown reduced the ability of tumor-initiating stem-like cells to induce liver cancer. These findings underscore the selective overexpression of OGC as an adaptive mechanism of HCC to provide adequate mGSH levels in the face of mt-cholesterol loading and suggest that OGC may be a novel therapeutic target for HCC treatment.

Abbreviations: DIC, dicarboxylate carrier; GSHEE, GSH ethyl ester; HCC, hepatocellular carcinoma; OGC, 2-oxoglutarate carrier; MOMP, mitochondrial outer membrane permeabilization; mGSH, mitochondrial GSH; mt-cholesterol, mitochondrial cholesterol; TICs, tumor-initiating stem like cells

* Corresponding authors at: Department of Cell Death and Proliferation, Instituto de Investigaciones Biomédicas de Barcelona, Consejo Superior de Investigaciones Científicas, 0803 Barcelona, Spain
E-mail addresses: cgrbam@iibb.csic.es (C. Garcia-Ruiz), checa229@yahoo.com (J.C. Fernández-Checa).
[1] Present address: The Francis Crick Institute, London, UK.
[2] Present address: Medical Oncology Department. Dana-Farber Cancer Institute, Harvard Medical School, Bringham and Women's Hospital, Boston, MA.
[3] Joan Montero and Nuria Matias contributed equally to the work

http://dx.doi.org/10.1016/j.redox.2017.08.022
Received 16 July 2017; Received in revised form 21 August 2017; Accepted 24 August 2017
Available online 14 September 2017

1. Introduction

Aberrant regulation of cholesterol homeostasis is associated with multiples cancer types. Cancer Genome Atlas (TCGA) database revealed a correlation between cholesterol synthesis and decreased survival in patients with cancer, including hepatocellular carcinoma (HCC) [1]. Of particular interest due to its low abundance is the pool of mitochondrial cholesterol (mt-cholesterol), which accumulates in different cancer cells. Increased mt-cholesterol contributes to chemotherapy resistance, decreases cell stress and cytochrome c release from mitochondria, increases resistance to large amplitude swelling and impairs proton leak [2–4]. Moreover, mt-cholesterol loading impaired the pore-forming activity of Bax by reducing mitochondrial outer membrane permeabilization (MOMP) [3–6]. The presence of cholesterol in liposomes mimicking MOM composition decreased the ability of Bax to integrate into the bilayer, impairing its permeabilization caused by oligomerized Bax or tBid-mediated Bax activation, effects that were reversed by fluidizing agents, thus underscoring a critical role of cholesterol-mediated changes in membrane dynamics in MOMP [3–6].

While these findings indicate that mt-cholesterol plays an anti-apoptotic role, mt-cholesterol accumulation sensitizes primary mouse hepatocytes, neurons or macrophages to TNF/Fas, amyloid-β peptide or anthrax lethal toxin-induced cell death, which is accompanied by mitochondrial GSH (mGSH) depletion due to cholesterol-induced impairment in mGSH transport [7–11]. The role of mt-cholesterol in promoting cell death is mediated by mGSH depletion, as its selective pharmacological decrease per se reproduced the sensitization seen after mt-cholesterol loading, while mGSH recovery protected against cell death [9,12]. Unlike cytosol, mitochondria do not synthesize GSH *de novo* from its constituent aminoacids and hence mGSH originates from the transport of cytosolic GSH into mitochondria by a carrier-specific process exhibiting two kinectic components [13]. Dicarboxylate (DIC) and 2-oxoglutarate (OGC) carriers are members of the mitochondrial carrier SLC25 family that exchange specific metabolites between cytosol and mitochondria. Although the transport of mGSH is not full understood, a wealth body of evidence from reconstitution assays in proteoliposomes, substrate specificity, kinetics, dependence on membrane potential and sensitivity to carrier-selective inhibitors indicated a putative role for DIC and OGC in the mitochondrial transport of GSH in kidney, liver, brain and colonic epithelial cells [14–17]. Moreover, functional expression in *Xenopus laevis* oocytes microinjected with OGC cRNA from HepG2 cells conferred mGSH transport activity that exhibited mutual competition with 2-oxoglutarate (2-OG) and sensitivity to phenylsuccinate [18]. Furthermore, the transport activity of OGC from rat liver was sensitive to cholesterol-mediated changes in membrane dynamics, thus reproducing the dependence of mGSH transport on membrane fluidity [7,18].

As a critical antioxidant, mGSH regulates the mitochondrial generation of reactive oxygen species (ROS), in particular the elimination of hydrogen peroxide produced from superoxide anion dismutation within mitochondria [17,19,20]. Cardiolipin is an important anionic phospholipid of the mitochondrial inner membrane that plays a key role in mitochondrial physiology and cell death regulation. Due to its four unsaturated acyl chains, cardiolipin is highly susceptible to ROS-mediated peroxidation, an event that is regulated by antioxidants, including mGSH [12,21]. Peroxidized cardiolipin (CLOOH) regulates critical steps in cell death, including the availability of unbound form of cytochrome c and MOMP and has emerged as a target for redox therapy in brain injury [12,22,23].

HCC is the most common form of liver cancer and as the end-stage of prevalent chronic liver diseases HCC is a leading cause of cancer-related deaths in the world. Since the role of OGC and DIC in HCC has not been previously examined, the purpose of our study was to characterize the expression of OGC and DIC in HCC and their role in the regulation of mGSH in HCC cells and impact in liver tumorigenesis.

2. Materials and methods

2.1. Cell culture, treatments and mitochondrial preparation

The human HCC cell lines, HepG2, Hep3B, the rat hepatoma cell line, Reuber H35, and the rat glioblastoma C6 cell line were obtained from the European Collection of Animal Cell Cultures. Rat liver and brain mitochondria were isolated by differential centrifugation and Percoll gradient, as previously described [8,19]. Mitochondria from HCC cells and human liver samples were obtained by rapid centrifugation through Percoll density gradient, as described previously [3]. In some cases, the mitochondrial suspension was incubated with 2-(2-methoxyethoxy) ethyl-8-(cis-2-*n*-octylcyclopropyl) octane (A_2C, 125 nmol/mg protein) for 30 min, as described in detail [24], and HCC cells were subjected to hypoxia (1% O_2) or treated with dimethyloxalylglycine (DMOG) (0.5–1 mM) for 6–12 h.

2.2. Human HCC samples and immunohistochemistry

Human liver samples were obtained from liver explants of patients diagnosed with HCC undergoing liver transplantation. The clinical data of the patients are presented in Supplemental Table 1. In addition, normal liver tissue was obtained from the surgical specimen of donor livers used for transplantation. The protocol was approved by the Hospital Clinic/UB Ethics Committee. Liver tissue was formalin-fixed and paraffin-embedded sections were cut for OGC or DIC immunostainning. Liver sections were incubated with anti-OGC (SC160804, Santa Cruz) or anti-DIC (TA331226 ORIGENE) antibodies (1:250) overnight, washed 3 times with PBS and incubated with secondary antibody (Vectastain antiGoat IgG biotinylated antibody). Slides were developed with ABC/HRP Complex and incubated with 1:10 DAB/hydrogen peroxide and counterstained with hematoxylin.

2.3. Silencing of OGC or DIC by siRNA

The siRNA-targeting OGC (human HSS112214 and HSS112215 and rat RSS343480 and R RSS34348079) and DIC (human Sc-93937 and HSS141712 and rat RSS332127 and RSS332128) as well as scrambled siRNA (sc-37007) were commercially purchased from Invitrogen, Inc and Santa Cruz Biotechnology, respectively. Transfection was performed using Lipofectamine2000 (Invitrogen). Briefly, 5×10^5 HepG2 cells or H35 cells were incubated with the transfection mixtures containing 60–80 pmol of the siRNA-targeting OGC or the scrambled control siRNA. Cells were assayed 48 h after transfection for mRNA and protein OGC levels and for GSH levels.

2.4. Extracellular flux analyses

In vivo real-time mitochondrial respiration (OCR) and glycolytic rate (ECAR) were monitored with the Seahorse XF24 Flux Analyser (Seahorse Bioscience) according to the manufacturer's instructions. Hep3B cells targeted with either SCR or OGC siRNA were seeded at 50,000 cells/well density in 24-well plates for 1 h in complete DMEM (10% FBS, 1% P/S) to allow adherence to the plate. For assessment of the real-time ECAR, cells were incubated with unbuffered assay media (XF Media Base containing 2 mM L-Glutamine) followed by a sequential injection of 10 mM glucose, 2 μM oligomycin and 50 mM 2-deoxyglucose. For OCR cells were incubated with unbuffered assay media (XF Media Base with 25 mM glucose, 4 mM L-glutamine and 5 mM pyruvate) followed by a sequential injection of 2 μM oligomycin, 0.2 μM carbonyl cyanide 4-(trifluoromethoxy) phenylhydrazone and 2 μM antimycin A plus Rotenone. Both ECAR and OCR measurements were normalized to ug of total protein following Bradford protein assay.

2.5. Mitochondrial network complexity analysis

Immunohistochemistry for the mitochondrial marker TOM20 was performed and analyzed using the ImageJ software. Briefly, acquired images were segmented by threshold to select the cellular area of study. TOM20 staining was submitted to background subtraction and filtering processes with Gaussian Blur filter set at 0.8. Segmentation of mitochondria was performed by local standard threshold using a radius of 7. Mitochondria were then subjected to particle analysis for acquiring aspect ratio (AR = major axis/minor axis) and circularity (4πxarea/perimeter^2). Form factor (FF) was calculated as the inverse of circularity. An AR value of 1 indicates a perfect circle, and as mitochondria elongates and become more elliptical AR increases. A FF value of 1 corresponds to a circular unbranched mitochondrion, while higher FF values indicate a longer more branched mitochondria. Particles smaller than 1.2 mm^2 were excluded. Images were taken with a Leica TCS SP5 laser scanning confocal system with a 633 oil immersion objective APO CS numerical aperture 1.4 equipped with a DMI6000 inverted microscope. GFP and AlexaFluor 594 images were acquired sequentially using 488, 594 nm laser lines, an acousto optical beam splitter and emission detection ranges 500–550, 605–700 nm, respectively. The confocal pinhole was set at 1 Airy unit. Pixel size was 60 nm. 43 X zoom was used in all images.

2.6. Mitochondrial RT2 profiler

The rat mitochondrial RT2 Profiler PCR array system (SABiosciences, Qiagen) was used for expression profiling of mitochondrion-focused genes in H35 cells vs rat liver. Total RNAs were isolated using TRIzol reagent (Life Technologies) and further purified with a Qiagen RNeasy minikit (catalog no. 74104). First-strand cDNAs were synthesized using an RT2 first-strand kit (catalog no. C-03; SABiosciences) following the manufacturer's protocol. The StepOnePlus real-time PCR system (Applied Biosystems) was used for the mitochondrion-focused PCRarray using RT2SYBR green/ROXqPCR mastermix (catalog no. PA-012; SABiosciences) and an RT2 Profiler PCR array kit (catalog no. PAMM-087C-2; SABiosciences).

2.7. Multicellular spheroids generation

Hep3B cell suspension containing 10,000 cells (200 µl) was added to each well of poly-HEMA-coated 96-well plates. Wells were overfilled with media to acquire a convex surface curvature and plates were inverted to allow cells to sediment to the liquid–air interface. Plates were returned to normal after 24 h incubation and excess media was removed by aspiration. Spheroid formation and growth was followed over 6–7 days with optical microscopy. In some cases, spheroids were stained with PCNA, Ki7, DHE and active caspase 3.

2.8. Stably OGC knockdown in Hep3B cells and TICs

Human OGC carrier (NM_003562) was stably silenced in Hep3B cells using previously validated commercial shRNA lentiviral plasmids (pLKO.1-puro) (Sigma Aldrich). OGC and control shRNA-transfected Hep3B cells were selected by puromycin exposure (2 µg/ml) and OGC silencing verified by western blot and qPCR. For stably OGC knockdown in tumor-initiating stem-like cells (TICs), we used two OGC (V3LMM_507075, V3LMM_507076) shRNAs in the lentiviral vector pGIPZ (Thermo Scientific). Lentiviral generation was performed by transfecting HEK293T cells with lentiviral vector, PMD2G (packaging vector), and psPAX2 (envelope vector) using BioT (Morganville Scientific) for 48-h. Concentrated virus was added to TICs, and cells were selected with Puromycin (10 µg/ml).

2.9. Subcutaneous and orthotopic HCC models

Male Balb/c athymic nude mice were kept under pathogen-free conditions with free access to standard food and sterilized water. The Hospital Clinic and UB Ethics Committee approved the animal protocols and procedures used for the present study. Hep3B cells (1×10^6 in 200 µl of PBS) were injected subcutaneously into the flanks of the mice. Differences in tumor volume were measured with a vernier caliper, and the volume was calculated as length x width^2 $\times$ 0.5. After sacrifice of the mice, tumors were fixed and paraffin sections (5 µm) from each area were stained with TUNEL staining using a commercial kit (In Situ Cell Death Detection Kit, POD from Roche). Immunohistochemical staining of CD34 was performed with rat monoclonal anti-CD34 antibody (Abcam, Cambridge, MA) at a dilution of 1:50 (2 µg/ml). The slides were examined with a Zeiss Axioplan microscope equipped with a Nikon DXM1200F digital camera.

For orthotopic HCC model, NOD/Shi-*scid/IL2r*$^{-/-}$ (NOG) mice were anesthetized with ketamine (50–80 mg/kg; ip) and xylazine (10 mg/kg; ip) and the left liver lobe was gently pulled out of the incision and immobilized onto moistened gauze. Using a 28 G 1cc U-100 insulin syringe, 50µl suspension of 10×10^5 of TICs stably transfected with SCR or OGC-shRNA was slowly injected into the parenchyma of the left lobe. After placing the lobe into the abdominal cavity, the peritoneum and abdominal muscle were closed and mice were administered buprenex (0.02–0.05 mg/kg; SC) for 48 h.

2.10. Statistical analyses

Results were expressed as mean ± SEM. Statistical significance of mean values was assessed using Student *t*-test and one-way ANOVA followed by Tukey post-hoc test. Statistics were performed using GraphPad Prism 6 software. $p \leq 0.05$ was defined as statistically significant.

3. Results

3.1. Cancer cells paradoxically maintain mGSH levels despite mitochondrial cholesterol accumulation

The pool of mGSH originates from the transport of newly synthesized cytosolic GSH by a carrier-dependent process [13,18], which is sensitive to cholesterol-induced decrease in membrane fluidity [7,10]. Hence, we examined the relationship between cholesterol and GSH in purified mitochondrial fractions from HCC cells (Supplementary Fig. 1A). Mitochondria from rat (H35) and human (HepG2) HCC cells exhibited increased cholesterol content compared to mitochondria isolated from rat or human liver of which > 80% was unsterified (Supplementary Fig. 1B). Unexpectedly, mGSH levels from HCC cells were similar to those found in mitochondria from non-tumor tissues (Supplementary Fig. 1C). Similar findings were observed in the Hep3B cells (not shown), which do not express p53, suggesting that increased mt-cholesterol and maintenance of mGSH is independent on the p53 status. Moreover, mitochondria from the rat glioblastoma cell line C6 displayed increased mt-cholesterol accumulation and similar mGSH levels compared to mitochondria isolated from rat brain (Supplementary Fig. 1B, C).

To examine if the ability of cancer cells to maintain mGSH results from the insensitivity of mGSH transport to cholesterol-mediated changes in membrane dynamics, we first determined the initial rate of transport of [^{3}H]-GSH at low (1 mM) and high (10 mM) concentrations in mitochondria from HCC cells. In line with previous findings [25], the transport of GSH was linear for 30 s and the initial rate of [^{3}H]-GSH transport in isolated mitochondria from H35 cells at both concentrations was similar to that seen in mitochondria from rat liver (Supplemental Fig. 1D), indicating the ability of HCC mitochondria to transport GSH despite increased mt-cholesterol. Although there was a

trend for lower initial transport of GSH at 10 mM in mitochondria from H35 compared to rat liver mitochondria, this outcome was not significant and together with the rate of transport at the lower GSH concentration suggests that the mitochondrial GSH transport through the high and low affinity sites is unaltered in H35 mitochondria despite significant mitochondrial cholesterol accumulation. Moreover, further enrichment of mitochondria from H35 and HepG2 cells with cholesterol (1.9 and 1.7-fold, respectively) following incubation with a cholesterol-BSA complex decreased the initial rate of [^{3}H]-GSH transport at low and high GSH concentrations (Supplementary Fig. 1E). Fluidization of mitochondria from H35 cells with the fatty acid derivative A_2C, which decreased the membrane order parameter (Supplemental Fig. 1F), further increased the initial rate of [^{3}H]-GSH (Supplemental Fig. 1G). Collectively, these findings indicate that HCC cells maintain physiological mGSH despite the sensitivity of mGSH transport to cholesterol-mediated changes in membrane fluidity.

3.2. Divergent expression of OGC and DIC in HCC cells and liver explants from patients with HCC

To identify underlying mechanisms for the paradoxical mGSH transport in HCC, we examined the expression of putative mGSH carriers, OGC and DIC. As seen, H35 and HepG2 cells exhibited higher expression of OGC compared to their corresponding normal tissues (Fig. 1A, B). Moreover, immunohistochemical staining revealed increased expression of OGC in tumor samples from liver explants of patients with HCC compared to control liver specimens (Fig. 1C; Table S1). In contrast to these findings, DIC expression decreased in both HCC cell lines and in human HCC samples compared to control counterparts (Fig. 1A, B, D). To examine whether other genes related to mitochondrial function are also differentially expressed in HCC, we performed quantitative RT-PCR analyses using a mitochondrial RT^2 Profiler PCR array that targets mRNAs of genes involved in mitochondrial function, biogenesis, and small molecule transporters (Fig. 1E). Among them, 23 genes were differentially regulated more than 50%, including 8 members of the SLC25 family of which *SLC25A17* (the peroxisomal transporter) and *SLC25A4* (a member of the adenine nucleotide translocase) were significantly overexpressed in H35 cells vs. rat liver (Fig. 1E). Interestingly, although the array did not contain *SLC25A11*, the expression of *SLC25A10* (DIC) was significantly decreased in H35 cells compared to rat liver, consistent with its downregulation in HCC cells and human liver samples (Fig. 1A, B, D).

To address potential mechanisms contributing to the increased expression of OGC in HCC cells, we examined the effect of hypoxia, which is known to mediate key changes in cancer cell metabolism. Hypoxia (1% O_2) increased the expression of HIF-1α and PDK1, a HIF-1α target gene, and this outcome paralleled the upregulation of OGC levels (Fig. 1F). Moreover, DMOG, a chemical hypoxia trigger, stabilized HIF-1α and reproduced the effect of 1% O_2 on OGC upregulation (Fig. 1F) and this effect was ameliorated by HIF-1α downregulation by siRNA (Supplementary Fig. 1H), suggesting that hypoxia induced OGC by a mechanism dependent on HIF-1α. Moreover, roxadustat (FG-4592), a small-molecule inhibitor of the HIF hydroxylating enzyme PHD, reproduced the effect of hypoxia or DMOG in OGC expression (not shown). Thus, our findings reveal the upregulation of OGC in HCC involving a HIF-1α-dependent mechanism.

3.3. OGC downregulation depletes mGSH levels and sensitizes HCC cells to hypoxia-induced oxidative stress and cell death

Given the divergent expression of OGC and DIC in HCC, we next addressed the relative contribution of both carriers in the maintenance of mGSH. Transfection of HCC cells with siRNAs targeting OGC did not affect DIC expression but effectively decreased OGC mRNA and protein levels (Fig. 2A), resulting in significant mGSH depletion compared to cells transfected with scrambled control siRNA (Fig. 2B). However, OGC siRNA treatment did not affect total GSH levels in either HCC cell line (21–25 nmol/mg prot and 19–24 nmol/mg prot GSH in SCR siRNA and OGC siRNA, respectively), effects that are in line with the lack of effect of OGC silencing by siRNA in the expression of GCL or GS, which are responsible for the *de novo* synthesis of GSH from its constituent aminoacids (not shown). Consistent with the lower expression of DIC compared to OGC, DIC silencing did not have a significant effect on mGSH levels (Supplemental Fig. 2), suggesting that HCC cells depend on OGC to maintain mGSH. Incubation with GSH ethyl ester (GSHEE), a permeable form of GSH which freely crosses membrane bilayers and diffuses into mitochondria, replenished the levels of mGSH in both cell lines despite OGC silencing (Fig. 2B), in line with findings in Niemann Pick type C disease or nonalcoholic steatohepatitis characterized by increased mt-cholesterol levels [26,27]. As hypoxia is a bad prognostic factor and an inherent feature of solid tumor growth, which induces ROS generation from mitochondria [28–31], we next addressed the impact of OGC silencing in the susceptibility of HCC cells to hypoxia. As seen, hypoxia or OGC knockdown per se did not have a significant impact on the generation of ROS nor affected cell viability (Fig. 2C, D). However, OGC silencing potentiated hypoxia-induced ROS generation and cell death and these effects were reversed by mGSH replenishment with GSHEE (Fig. 2C, D). These findings indicate that OGC silencing sensitizes HCC cells to hypoxia by an oxidative stress-dependent mechanism.

3.4. OGC knockdown impairs cell proliferation in 3-D multicellular HCC spheroids

In view of the preceding findings, we next focused on the role of OGC in three-dimensional multicellular tumor spheroids, which represent an intermediate complexity model between in vitro monolayer cultures and in vivo tumors. Treatment with siRNA targeting OGC significantly downregulated OGC protein levels compared to SCR siRNA treatment (Fig. 3A), which translated in mGSH depletion (5.8 ± 1.4 nmols/mg protein and 2.6 ± 0.7 nmol/mg protein in SCR siRNA or OGC siRNA treated Hep3B spheroids, respectively). Time-dependent growth monitoring by microscopy and histology analyses indicated a significant reduction in the size of spheroids following OGC silencing compared to SCR siRNA treatment, indicating decreased growth rate (Fig. 3B, C). Moreover, GSHEE treatment significantly reversed the cell growth arrest following OGC knockdown (Fig. 3B). Consistent with these findings, scrambled SCR siRNA-treated spheroids exhibited a ring of cells positive for PCNA and Ki67 that was substantially reduced following OGC siRNA treatment, indicating reduced proliferation of Hep3B cells in the periphery of the spheroids (Fig. 3D). Staining with the hydroxyprobe pimonidazole to detect hypoxia areas revealed the growth of hypoxic cells in the core of the spheroids following SCR siRNA treatment, and this event was substantially reduced in OGC siRNA-treated spheroids, indicating that OGC silencing prevents hypoxic cell formation in 3-D spheroids (Fig. 3E). In line with findings in monolayer culture, OGC siRNA-treated spheroids exhibited increased DHE fluorescence compared to spheroids exposed to SCR siRNA (Fig. 3E), indicating increased ROS generation, while treatment with tetramethylrhodamine methyl ester revealed mitochondrial membrane depolarization in OGC siRNA-treated spheroids (Fig. 3F). Moreover, OGC silencing resulted in increased active caspase-3 fragment in the spheroids, pointing to pro-caspase-3 processing and activation (Fig. 3F). These findings indicate that OGC downregulation impairs cell growth and induces cell death in three-dimensional Hep3B spheroids.

3.5. OGC regulates mitochondrial oxygen consumption and glycolysis without alterations in mitochondrial morphology

In addition to the dependence on glycolysis, cancer cells maintain concomitant high mitochondrial oxidative phosphorylation rates for survival and ATP generation [32,33]. Therefore, we next examined the

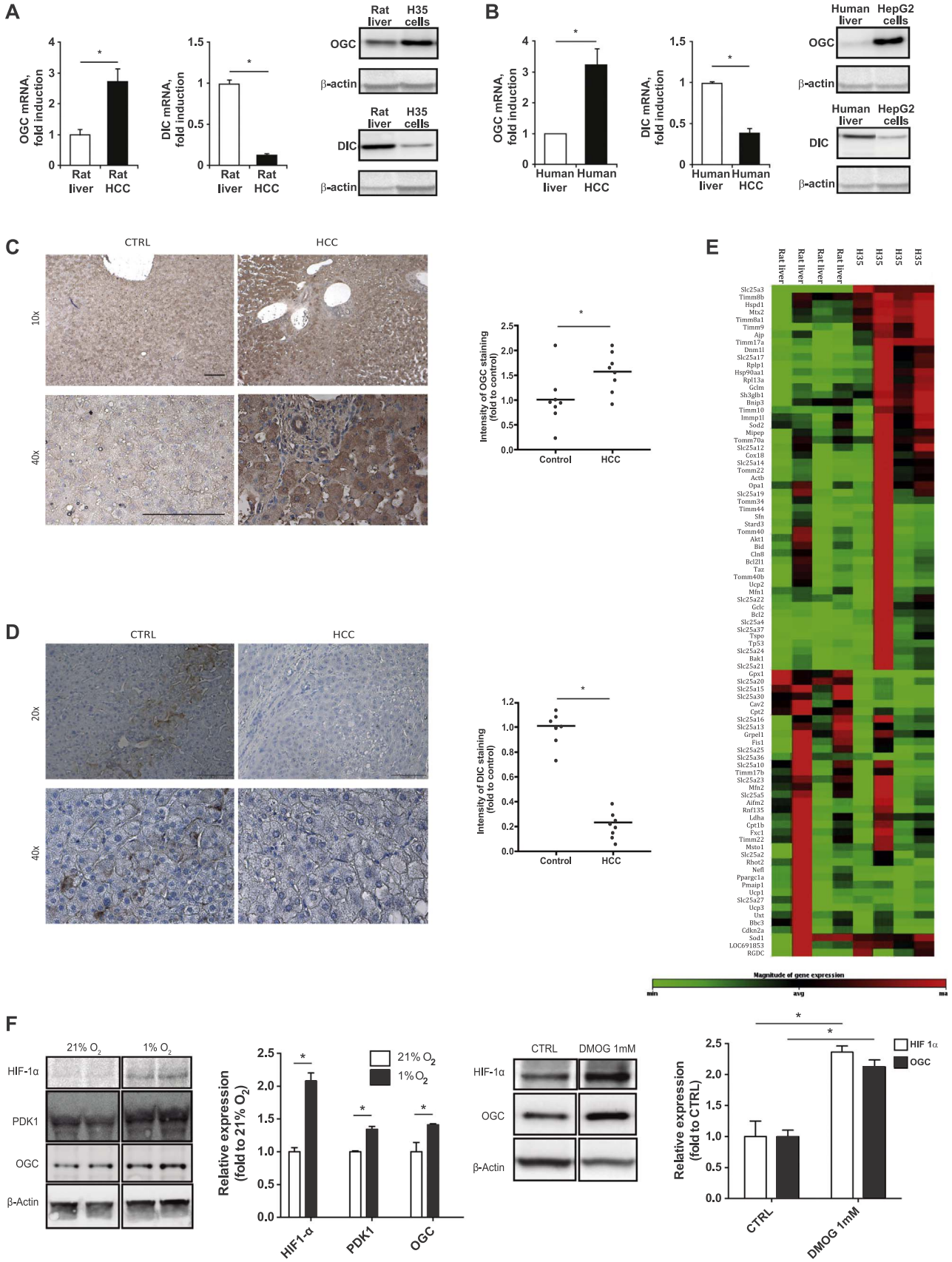

Fig. 1. OGC and DIC expression in HCC cells and human HCC. A, Protein and mRNA levels of OGC and DIC in rat liver and H35 cells. B, OGC and DIC expression at the mRNA and protein levels in human liver and HepG2 cells. C-D immunohistochemistry of OGC (C) and DIC (D) in liver explants from patients with HCC. Scale bar, 100 μm. E. Heat-map analyses of expression of genes involved in mitochondrial homeostasis and function in H35 cells vs rat liver. F, HIF-1α stabilization, PDK1 and OGC regulation in Hep3B cells incubated under 1% O_2 and effect of DMOG in HIF-1α and OGC regulation in Hep3B cells. Data represent mean ± SEM of 5–8 determinations. *$p < 0.05$ vs control.

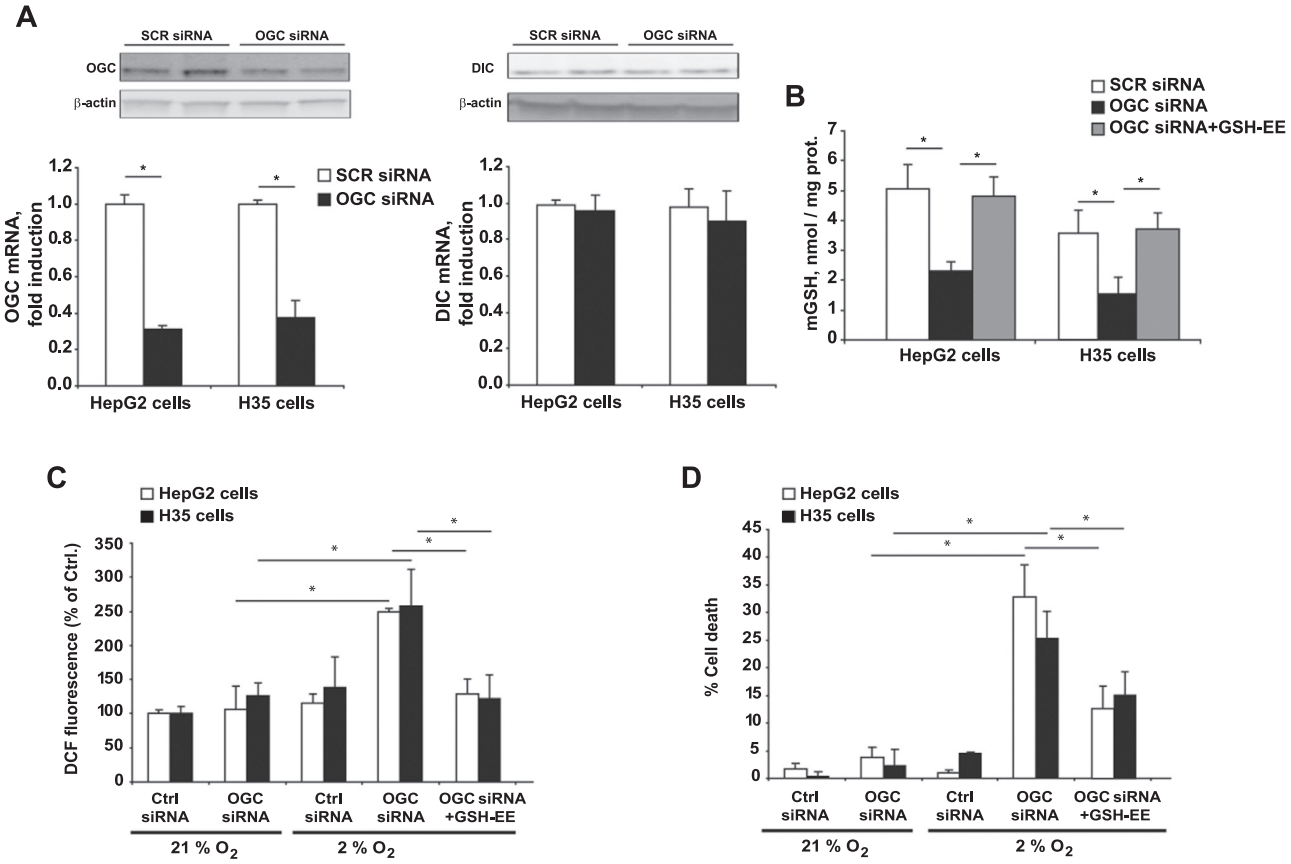

Fig. 2. OGC downregulation deplestes mGSH and sensitizes HCC cells to hypoxia-induced ROS generation and cell death. A, Expression of OGC at the mRNA and protein levels in H35 and HepG2 cells following siRNA treatment against OGC. The effect of OGC silencing is assessed on the expression of DIC. B, OGC downregulation results in mGSH depletion while GSH-EE treatment restores mGSH despite OGC silencing. C, DCF fluorescence to monitor ROS generation in cells subjected to hypoxia with or without OGC silencing by siRNA. In some cases, cells were pretreated with GSH-EE as in B. D, cell death following hypoxia and OGC silencing with or without GSH-EE. Data are mean ± SEM of 5 different experiments. *$p < 0.05$ vs. SCR siRNA treated cells.

role of OGC in mitochondrial oxygen consumption rates (OCR). Basal mitochondrial respiration in Hep3B cells was estimated by measuring OCR after subtraction of the residual oxygen consumption in the presence of antimycin A plus rotenone (Fig. 4A). As seen, OGC silencing decreased basal respiration in Hep3B cells (Fig. 4B). Moreover, maximal respiration determined by the addition of the protonophore FCCP to uncouple mitochondrial ATP generation from oxygen consumption decreased following OGC silencing compared to SCR siRNA treatment (Fig. 4C), and this effect was accompanied by decreased ATP production rate through oxidative phosphorylation (Fig. 4D). However, coupled respiration and spare respiratory capacity were unaffected by OGC silencing (Supplemental Fig. 3A, B). These effects were largely recovered by GSHEE treatment (Fig. 4A-D) to increase mGSH, consistent with previous observations indicating a key role of mGSH in the regulation of ATPase, complex IV activity and mitochondrial respiration [34,35]. Besides these effects on OCR, OGC silencing resulted in decreased extracellular acidification rate (ECAR) and reduced glycolytic capacity (Fig. 4E) that, unlike OCR, were refractory to GSHEE treatment, suggesting an irreversible oxidative inactivation in line with the redox-sensitive function of specific glycolytic enzymes [36,37]. Thus, OGC downregulation restricts ATP generation in Hep3B cells by impairing oxidative phosphorylation and glycolysis.

Since MISC-1, the *C. elegans* orthologue of mammalian OGC, has been shown to regulate mitochondrial fusion/fission [38], we next examined whether OGC modulates mitochondrial morphology. Confocal microscopy analyses following staining with TOM20 revealed similar mitochondrial morphology in SCR-siRNA and OGC siRNA-treated HCC cells (Fig. 4F). Moreover, determination of the aspect ratio from the major/minor axis, circularity and form factor revealed that OGC silencing did not affect mitochondrial morphology (Fig. 4F). In line with these findings, the expression level of proteins that regulate mitochondrial fusion such as mitofusin-1 and mitofusin-2 was similar between SCR and OGC siRNA-treated Hep3B cells, while the expression of Opa1 and phospho-DRP1 were somewhat reduced (Supplemental Fig. 3C). Electron microscopy analyses of H35 cells compared to rat liver and mitochondrial staining with mitotracker green with or without OGC silencing discarded alterations in mitochondrial morphology (Supplemental Fig. 3D).

3.6. OGC silencing promotes hypoxia-induced cardiolipin peroxidation, which reverses cholesterol-mediated inhibition of membrane permeabilization

Since mGSH regulates the oxidative status of cardiolipin and CLOOH promotes MOMP and cell death [12,22], we next examined the role of OGC on cardiolipin homeostasis and whether CLOOH, which modulates membrane biophysical properties, reverses cholesterol-mediated inhibition of membrane permeabilization [3,5,6]. High-performance thin layer chromatography indicated the presence of CLOOH, particularly its dihydroperoxide form, in OGC siRNA-treated Hep3B cells following hypoxia exposure compared to OGC silencing or hypoxia alone (Supplemental Fig. 4A, B). Moreover, mass spectrometry lipidomic analyses of cardiolipin fractions further indicated the oxidation of polyunsaturated cardiolipin species following OGC knockdown and hypoxia exposure (Supplementary Fig. 4C). This outcome, however, was not specific for cardiolipin peroxidation as the levels of other lipid hydroperoxides, including fatty acid hydroperoxides with conjugated dienes, increased as well (not shown), in line with findings of hepatic

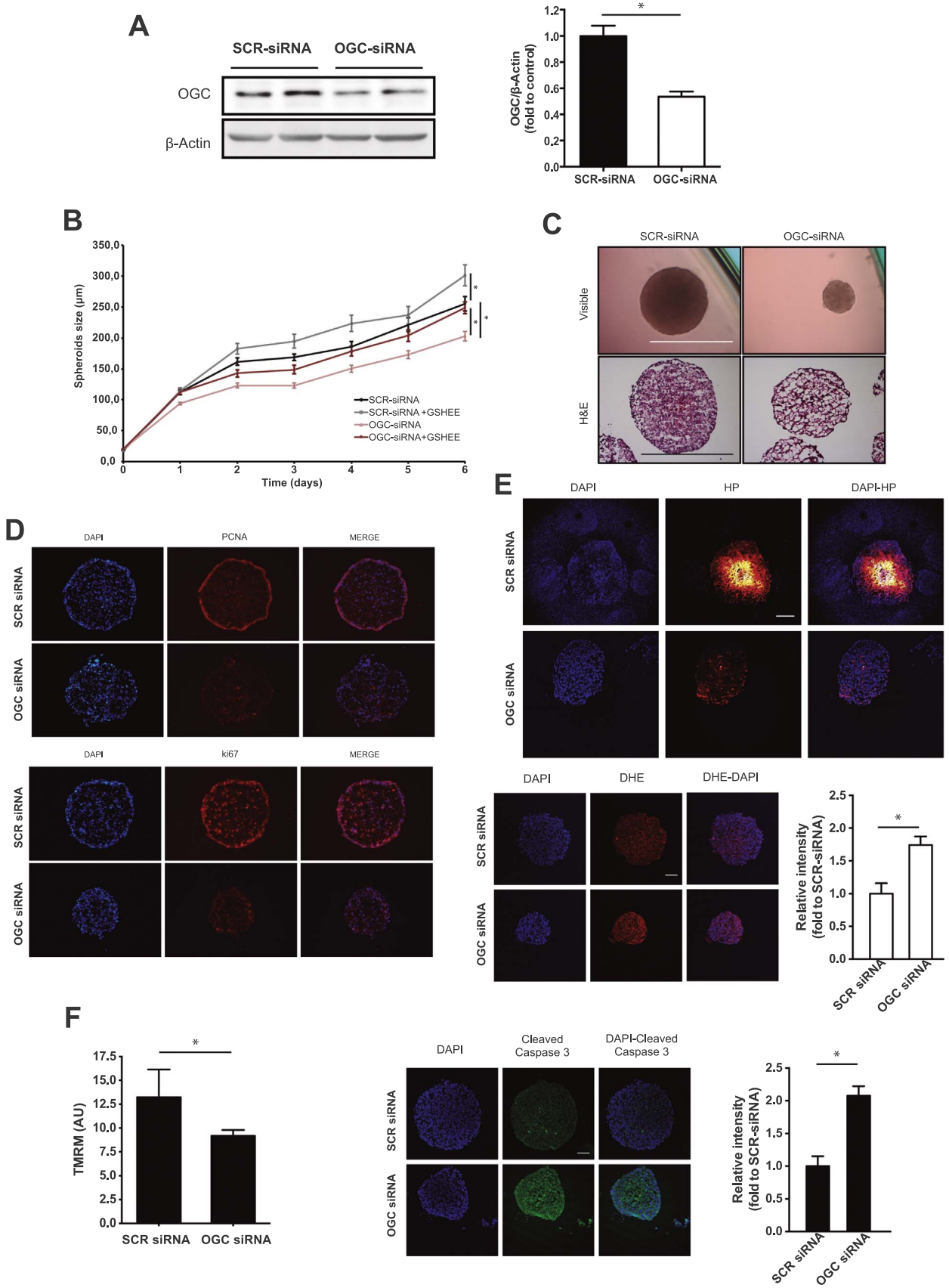

Fig. 3. OGC silencing impairs cell proliferation in 3-D multicellular HCC spheroids. A, OGC protein levels in Hep3B cells treated with siRNA. B, Hep3B spheroid size monitored over time with or without OGC downregulation and GSH-EE treatment. Data are mean ± SEM of n = 6–8. *p < 0.05 as indicated. C, Visible microscopy and histology analyses of Hep3B spheroids with or without OGC siRNA treatment. Scale bar, 100 μm. D. Hep3B spheroids were stained with PCNA or Ki67 to monitor cell proliferation. E, Hep3B spheroids stained with DAPI and hypoxyprobe pimonidazole to identify hypoxic areas or DHE to monitor ROS generation. Scale bar, 50 μm. Data are mean ± SEM of n = 6–8. *p < 0.05. F. Hep3B spheroids staining with TMRM to determine mitochondrial membrane potential and staining with antibody anti-cleaved caspase 3 and counterstained with DAPI. Data are mean ± SEM of n = 6–8. *p < 0.05.

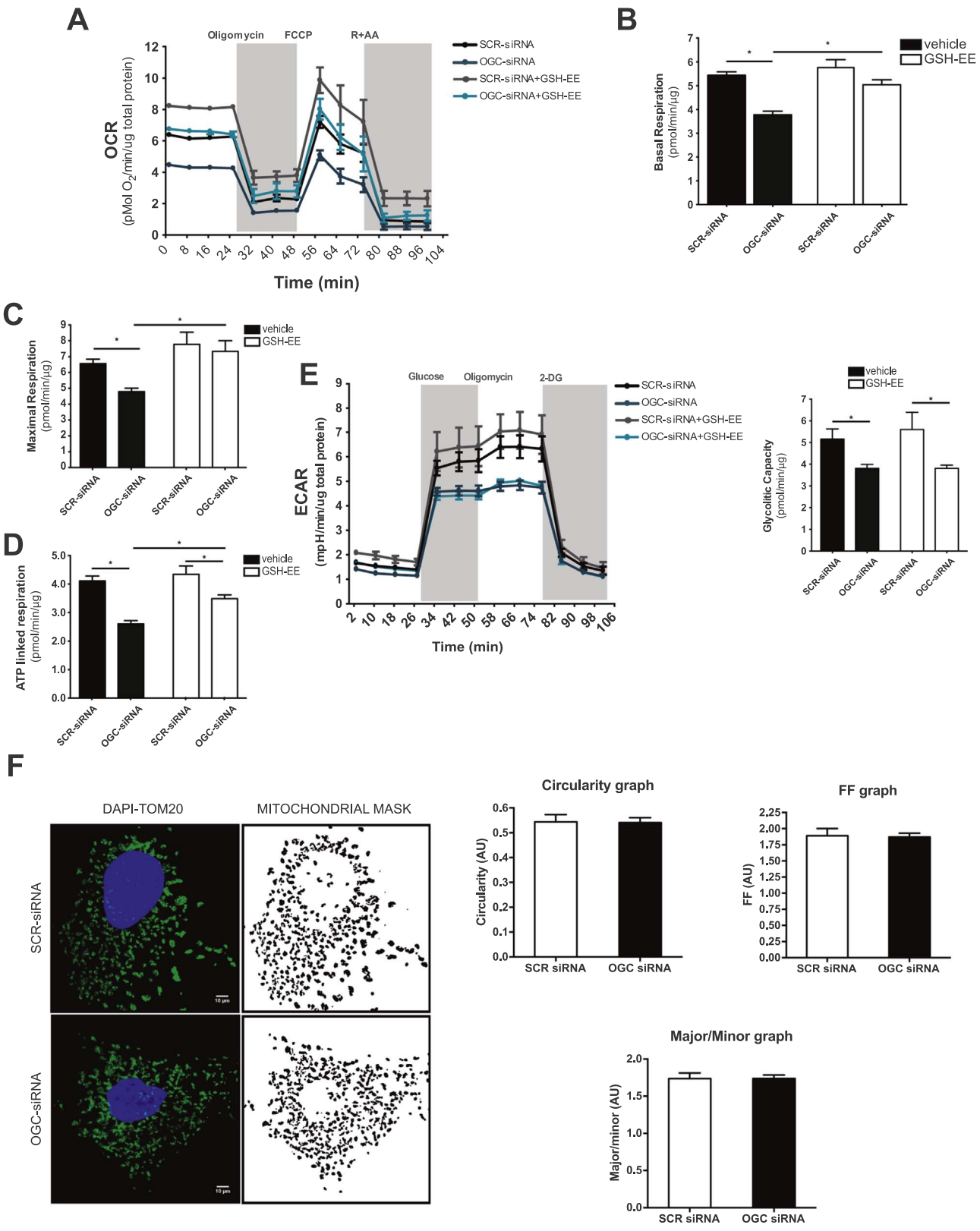

Fig. 4. OGC regulates mitochondrial oxygen consumption and glycolysis without alterations in mitochondrial morphology. A, Real-time OCR analyses of Hep3B cells with or without OGC silencing by siRNA and GSH-EE treatment. B-D, Determination of basal respiration, maximal respiration and ATP production of Hep3B cells following OGC silencing by siRNA with or without GSH-EE treatment. E, real-time ECAR analyses of Hep3B cells treated with siRNA against OGC with or without GSH-EE treatment, and determination of glyclytic capacity in Hep3B cells with or without OGC silencing and GSH-EE treatment. F, mitochondrial network complexity assay determined from TOM20-labelled mitochondria and examined by a laser scanning confocal microscope and analyzed with the ImageJ software to determine circularity, form factor and aspect ratio (major/minor axis). Data are mean ± SEM of n = 4–6 experiments. *p < 0.05 as indicated.

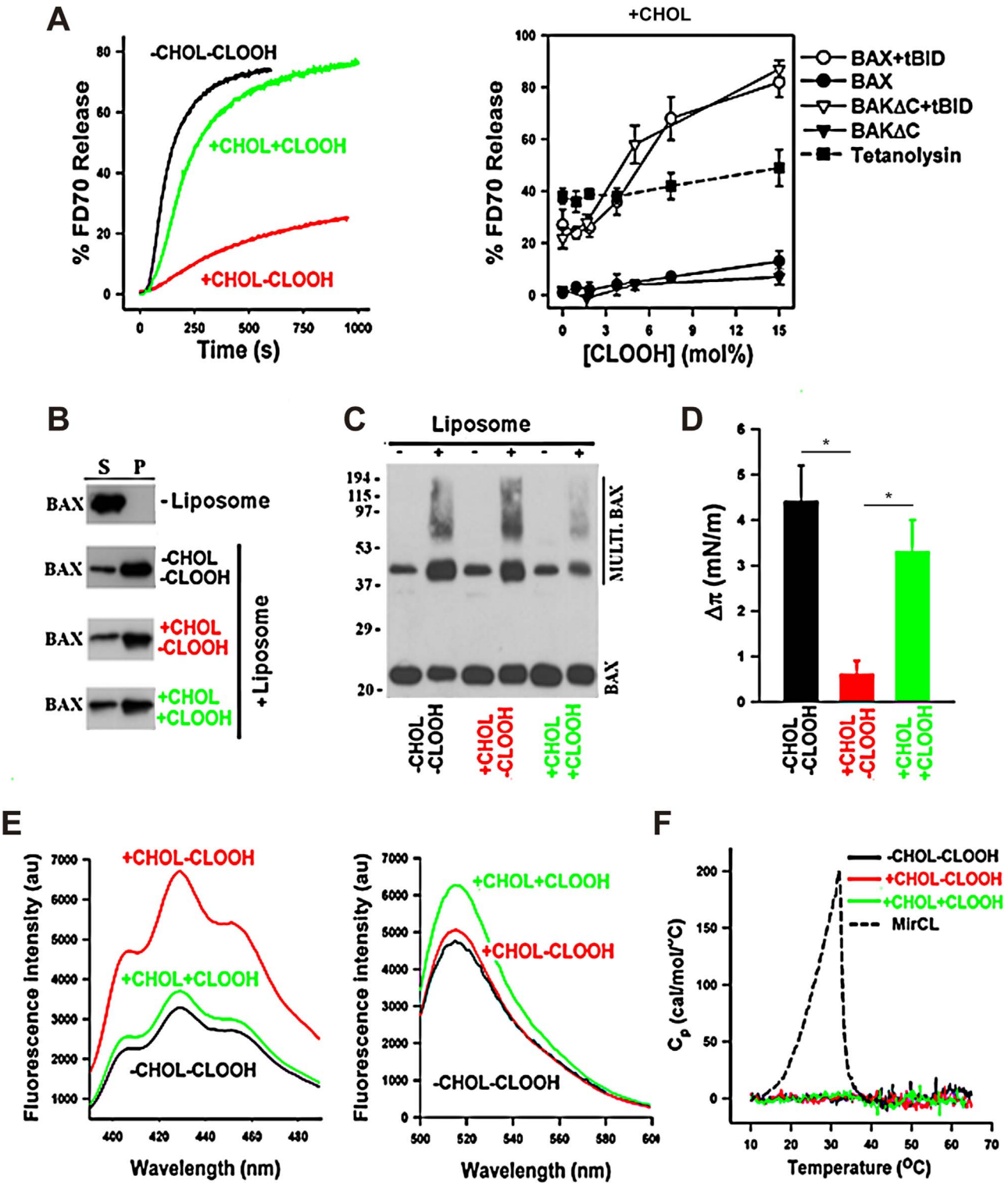

Fig. 5. OGC downregulation promotes hypoxia-mediated CLOOH, which reverses cholesterol-mediated inhibition of membrane permeabilization. A, Representative kinetics of BAX + tBID induced FD70 release from vesicle LUV composed of PC/CL (-CHOL-CLOOH), PC/CL/CHOL (+ CHOL-CLOOH), or PC/ CLOOH/CHOL (+ CHOL + CLOOH). BAX and tBID concentrations were 40 nM, and dose-dependence effects of CLOOH on LUV permeabilization induced by different pore-forming proteins in LUV composed of PC/CL/CHOL in which CL was substituted by indicated molar amounts of CLOOH. Concentrations of BAX, BAKΔC, tBID, and tetanolysin were 40 nM, 40 nM, and 3 nM, respectively. Data represent mean values and standard errors of 3–6 independent measurements. B-C, CHOL and CLOOH do not significantly affect BAX recruitment to liposomes (B) nor BAX oligomerization (C). BAX, monomeric BAX; Multi-BAX, oligomeric BAX. D, CLOOH reverses the inhibitory effect exerted by CHOL on the capacity of BAX to penetrate into lipid monolayers spread at 30 mN/m followed by addition of octylglucoside-oligomerized BAX (500 nM) into the subphase, and monolayer surface pressure increase was determined when the signal reached a plateau. Data represent mean values and S.E. of 3–4 independent experiments. E, CLOOH reverses the increase in the micropolarity of the lipid bilayer hydrocarbon core exerted by CHOL determined by polarization fluorescence emission spectra of indicated multilamellar vesicles containing 5 μM DPH incorporated. Excitation wavelength was 370 nm. All spectra were corrected by substracting the spectra of buffer, or spectra of phospholipid suspensions without fluorescent probe. Representative fluorescence emission spectra of 0.2 mol% F-DHPE incorporated in multilamellar vesicles of indicated lipid composition. Excitation wavelength was 480 nm. All spectra were corrected by substracting the spectra of buffer, or spectra of phospholipid suspensions without fluorescent probe. F, Representative thermograms obtained by differential scanning calorimetry for multilamellar vesicles of indicated lipid compositions. MirCL, 50 mol miristoyl cardiolipin plus 50 mol PC, a lipid mixture used as a positive control for lipid domain formation.

mGSH depletion by acute alcohol exposure [39]. However, we focused on the role of peroxidized cardiolipin species on bilayer permeabilization due to its role in membrane remodeling and apoptosis regulation [12,23,24]. To test if CLOOH antagonizes the inhibitory role of cholesterol on Bax apoptotic pore formation, we used a well-established minimalist system bearing physiological relevance, using liposomes whose lipid composition mimicked that of the mitochondrial outer membrane (MOM-like LUVs) entrapping large molecular weight fluorescent dextrans (FD70) followed by treatment with recombinant Bax and its activator ligand tBid. Consistent with previous studies, tBid-activated Bax induced fast and efficient release of FD70 from MOM-like LUVs, indicating the formation of large Bax apoptotic pores, whereas the presence of cholesterol markedly inhibited Bax-induced LUVs permeabilization (Fig. 5A). Furthermore, incorporation of CLOOH generated from the oxidation of cardiolipin in vitro by 2-2'-azo bis(2-amidinopropane) hydrochloride [12], reversed the inhibitory effect exerted by cholesterol on bilayer permeabilization elicited by Bax or BakΔC activated by tBid in a dose-dependent and specific manner, without effect on tetanolysin, a cholesterol-dependent pore-forming bacterial toxin (Fig. 5A). Bax apoptotic pore formation is linked to Bax membrane insertion and oligomerization. Previous studies showed that cholesterol specifically inhibits Bax apoptotic pore formation by blocking Bax membrane insertion [3,5]. Further biophysical and biochemical studies revealed that CLOOH did not affect the recruitment of Bax to liposomes nor its oligomerization (Fig. 5B, C), while CLOOH reversed the inhibition exerted by cholesterol on Bax membrane insertion and ability to penetrate in lipid monolayers (Fig. 5D). In our reconstituted system, cholesterol and CLOOH exhibited an opposite effect on the micropolarity of the lipid bilayer hydrocarbon core (Fig. 5E), although compared to myristoyl cardiolipin (MirCL) they did not affect the general organization of membrane lipids into large-scale domains (Fig. 5F). Thus, OGC knockdown following hypoxia promotes CLOOH, which in turn, antagonizes cholesterol-mediated inhibition of membrane permeabilization.

3.7. Genetic OGC knockdown decreases liver cancer

To examine the relevance of the preceding findings, we used an orthotopic model of HCC induced by the injection of TICs with or without shRNA-mediated OGC knockdown in NOG mice. TICs ($CD133^+/CD49f^+$) are characterized by the expression of the pluripotency marker Nanog and TLR4 [40]. TICs transfected with lentiviral-mediated shRNA targeting OGC exhibited significant reduced expression of OGC compared to SCR shRNA-treated TICs (Fig. 6A). Although OGC downregulation markedly reduced cell number, the viability of transduced TICs remained unchanged and exhibited increased cell size (Fig. 6B). Moreover, this outcome did not compromise the stemness phenotype of transduced TICs as revealed by the expression of Nanog and TLR4 (Fig. 6C). To examine the role of OGC on the tumorigenic potential of TICs, SCR shRNA or OGC shRNA-transfected TICs were injected in the left liver lobe of NOG mice. While engrafted SCR shRNA TICs led to macroscopic appearance of liver tumors, the injection of OGC shRNA TICs resulted in a dramatic reduction in tumor weight and volume without change in tumor density, leading to reduced liver/body weight ratio (Fig. 6D). Histology analyses of liver sections from mice injected with OGC shRNA TICs indicated preserved liver architecture compared to liver samples from mice treated with SRC shRNA TICs (Fig. 6E). Moreover, this outcome was accompanied by the reduction of PCNA and increased TUNEL staining in liver tumors from mice injected with OGC shRNA TICs (Fig. 6E). Similar findings were observed in Hep3B cells stably transduced with shRNA against OGC and injected subcutaneously in the flanks of nude mice. OGC silencing in Hep3B cells resulted in significant downregulation of OGC RNA levels and depletion of mGSH (Supplementary Fig. 5A, B). Tumor volume was significantly reduced in nude mice xenografted with OGC shRNA Hep3B cells compared to SCR shRNA Hep3B controls (Fig. 6F), despite staining with anti-CD34 antibody indicative of microvessel formation (Supplemental Fig. 5C).

As mGSH depletion by OGC downregulation (Fig. 2) indicates impaired exchange between cytosolic GSH and mitochondrial 2-OG [15], we next addressed whether the impact of OGC knockdown in restraining liver tumor growth could reflect alterations in 2-OG-dependent histone demethylases through changes in cytosolic 2-OG. HCC cells with or without OGC downregulation with siRNA were fractionated into cytosol and mitochondria to determine 2-OG levels. As seen, OGC siRNA treatment significantly depleted 2-OG in the cytosolic fraction (Supplementary Fig. 5D). Expression of the jumonji-domain histone demethylases JMJDs in cell and nuclear extracts and the activity of the JMJ2 histone demethylase were unchanged following OGC silencing (Supplementary Fig. 5E, F). Taken together, these findings indicate that OGC promotes in vivo liver tumorigenesis independently of changes in histone demethylases.

4. Discussion

We investigated the role of mGSH transporters OGC and DIC in HCC. Our findings uncover a divergent expression of DIC and OGC in HCC cells and human HCC tumors, with selective OGC upregulation, whose silencing resulted in significant mGSH depletion. This outcome together with a minimal impact of DIC in mGSH homeostasis, likely reflecting its low abundance, indicate that HCC depend on OGC upregulation to maintain optimal mGSH levels despite cholesterol loading to promote HCC development (Fig. 7). Cancer cells exhibit increased ROS generation, which functions as signaling intermediates to promote proliferation and uncompromised cell growth. While this premise implies that antioxidants can prevent cancer progression, in line with preclinical studies [41,42], large randomized clinical trials have produced inconsistent results and recent studies demonstrated that antioxidants (e.g. NAC or vitamin E) accelerate cancer progression and increase metastasis in mice [43,44]. Thus, although cancer cells have increased metabolic ROS generation, they have a strong reliance on antioxidant defense not only to exploit the use of ROS as signaling molecules but also to prevent cell death from uncontrolled ROS generation and subsequent oxidative stress. This reliance in the ROS stress response determines the vulnerability of cancer cells to strategies that limit their antioxidant strategies. For instance, GSH depletion by piperlongumine, a natural product from the plant *Piper longum L*, triggers apoptosis and necrosis in leukemia cells without effect in primary normal cells [45], and increased GSH synthesis ameliorates oxidative stress in tumors with fumarate hydratase (FH) deletion [46]. Moreover, small molecules with anticancer potential (e.g. β-phenethyl isothiocyanate) kill cancer cells due to the rapid and selective mGSH depletion (35). Our findings indicating a link between hypoxia and OGC imply that OGC upregulation stands as an adaptive strategy for sustaining mGSH levels to control hypoxia-induced ROS generation and liver cancer promotion.

Although OGC is a component of the malate-aspartate shuttle that mediates the export of 2-OG by a dicarboxylate (e.g. malate) cumulating evidence from multiple tissues and cell lines using different approaches, such as reconstitution in proteoliposomes, functional expression, kinetics, substrate specificity and sensitivity to carrier-selective inhibitors, have provided evidence for OGC as a mGSH carrier [14–18,47]. Intriguingly, however, the expression of OGC in the cytoplasmic membrane of *Lactococcus lactis* (*L. lactis*) and subsequent fusion of *L. lactis* membrane vesicles with liposomes failed to show significant GSH transport activity [48]. While the relevance of this particular approach in relation to the existing body of data supporting a role of OGC in mGSH transport has been recently assessed [15], this finding contrasts with the functional expression of mitochondria-targeted OGC from HepG2 cells in *X.* oocytes and the reconstitution of partially purified OGC in proteoliposomes from kidney mitoplasts [18,46]. Whether the unexpected findings from Booty and colleagues [48]

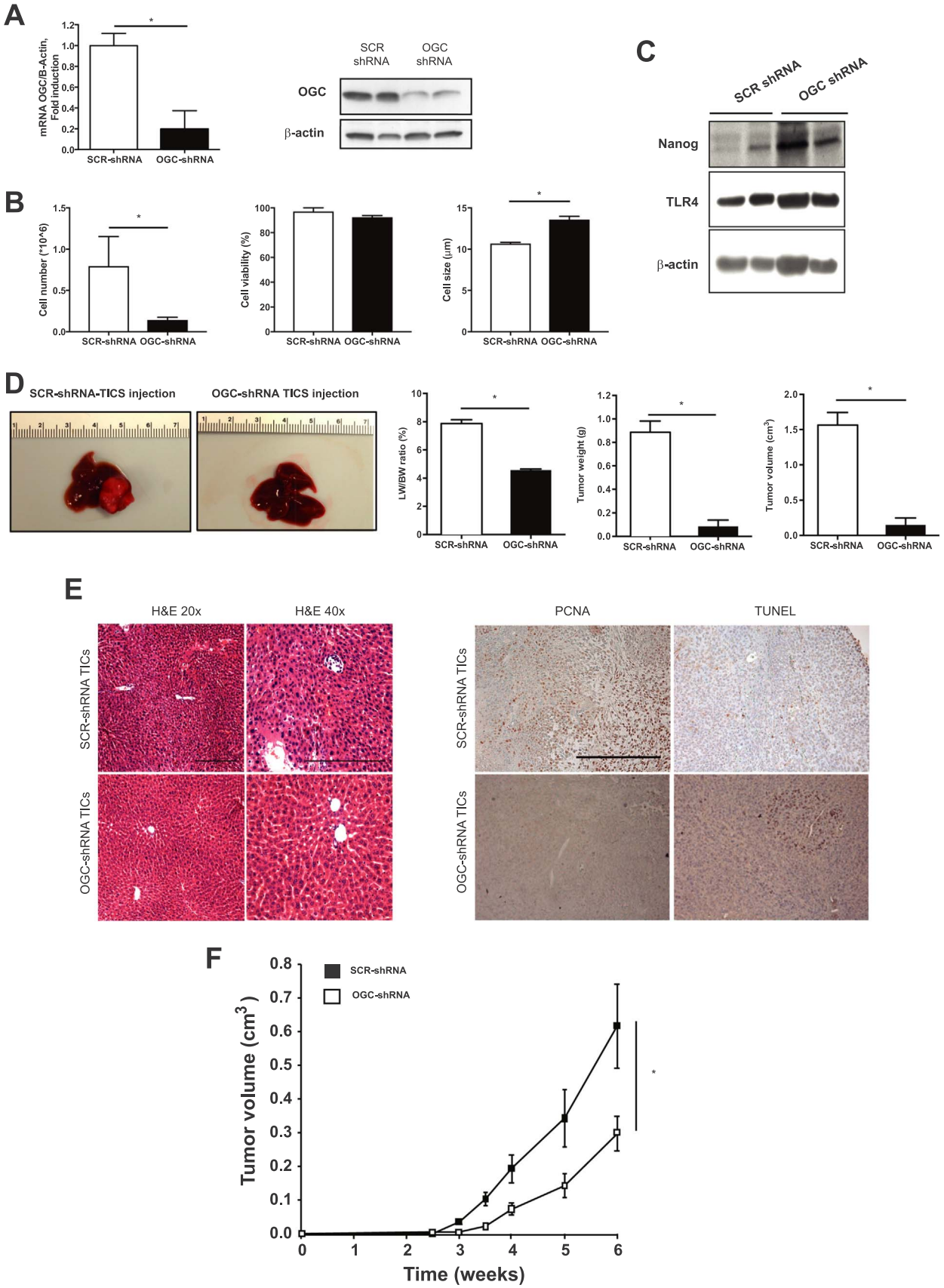

Fig. 6. Stably OGC knockdown reduces in vivo liver cancer induced by TICs. A, $CD133^+/CD49f^+$ TICs transfected with lentiviral-mediated shRNA decreased OGC mRNA and protein levels. B, Cell number, viability and cell size of TICs with or without shRNA transfection. C, Nanog and TLR4 expression of TICs with or without OGC knockdown. D, macroscopic appearance of liver from mice injected in the left lobe with SCR shRNA or OGC shRNA transfected TICs, and liver to body weight ratio, tumor weight and tumor volumen from livers of mice injected with SCR shRNA or OGC shRNA transfected TICs. E, Histology analyses of liver sections from mice injected with SCR shRNA or OGC shRNA transfected TICs and PCNA and TUNEL staining of liver samples from mice injected with SCR shRNA or OGC shRNA transfected TICs, Scale bar, 100 μm. F. Subcutaneous tumor volume induced by injection of Hep3B cells transfected with SCR shRNA and OGC shRNA. Data are the mean ± SEM of n = 4–5. *p < 0.05 vs SCR shRNA.

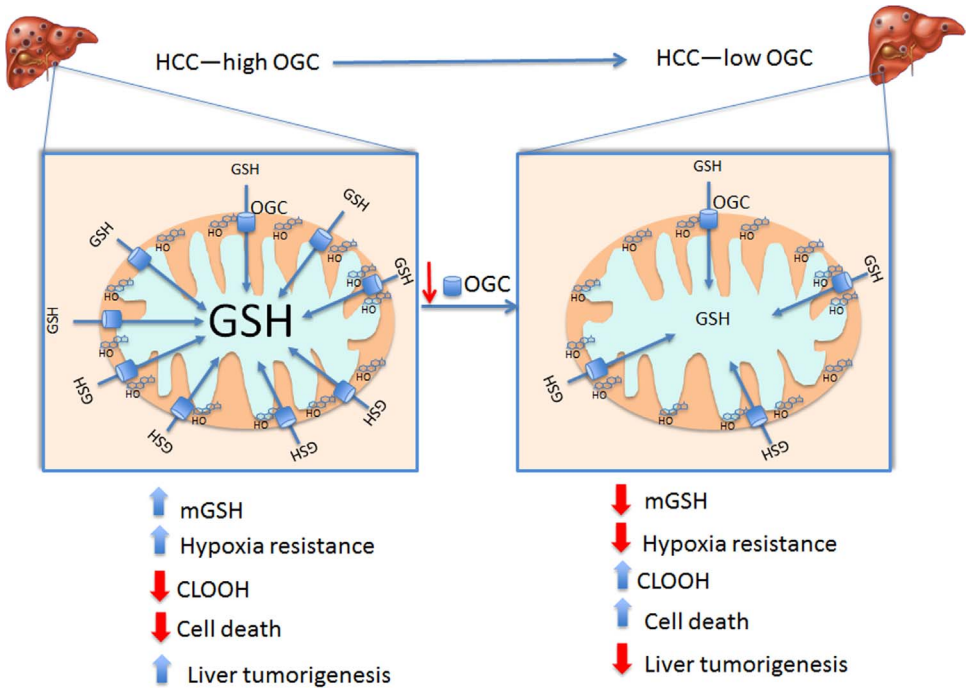

Fig. 7. Schematic representation of the role of OGC in HCC. HCC exhibit increased OGC expression, which overcomes the cholesterol-mediated impairment in mGSH transport, thus providing adequate mGSH levels. This increased state of mGSH defense protects against hypoxia-induced ROS generation and ensures cardiolipin status in its reduced form. This event along with the increased cholesterol accumulation in mitochondria protects against MOMP and promotes liver cancer. Knockdown of OGC antagonizes these events due to mGSH depletion, in line with the current view that cancer cells high a high reliance on antioxidants to control the fate of ROS generation to promote cancer development.

reflect specific biochemical and biophysical properties of cytoplasmic membrane vesicles from *L. Lactis* in which the OGC was reconstituted or if the putative function of OGC as a mGSH transporter in physiological settings requires other partners remains to be further investigated. Of relevance, previous findings indicated that the transport of 2-OG and GSH from rat liver mitochondria exhibit mutual competition and sensitivity to the OGC inhibitor phenylsuccinate, and more importantly, to cholesterol-mediated changes in membrane dynamics [18], indicating that OGC accounts for a key feature of hepatic mGSH transport. Moreover, the kinetic parameters of 2-OG transport from rat liver mitochondria are similar to the low-affinity component of the hepatic mGSH transport showing a Michaelis constant in the low mM range and similar maximum velocity, suggesting that OGC may account for the low-affinity transport of hepatic mGSH [13,18].

Our findings provide evidence that OGC silencing significantly depletes mGSH levels, sensitizing HCC cells to hypoxia-induced ROS generation and cell death as well as arresting growth in multicelular tumor cell spheroids, events that are reversed by mGSH replenishment with GSHEE. An important observation is the fact that OGC knockdown in HCC cells decreases OCR and ECAR, which are differentially regulated by GSHEE treatment. The fact that mGSH depletion negatively impacts mitochondrial OCR and glycolysis suggests an oxidative stress-dependent mechanism, consistent with previous findings showing the dependence of mitochondrial function and respiration on mGSH levels [34,35] and the susceptibility of critical cysteine residues of key glycolytic enzymes (e.g. M2 isoform of pyruvate kinase and GAPDH) to oxidatve inactivation [36,37]. The reduction in glycolysis by OGC silencing is insensitive to mGSH replenishment by GSHEE, which may reflect irreversible oxidation of cysteines 358 and 152 of pyruvate kinase M2 and GAPDH, respectively.

In line with previous reports, our results further support a link between mitochondrial metabolism and redox homeostasis through mGSH status and their relationship in cancer cell growth. For instance, glutamate dehydrogenase (GDH) downregulation has been shown to deplete 2-OG levels impairing the antioxidant enzyme GSH peroxidase 1, resulting in increased oxidative stress in lung and breast cancer cells [49]. Fumarate accumulation due to FH mutations associated with increased tumor cell growth, induces mGSH succination and hence mGSH depletion, which leads to a compensatory increase in GSH neosynthesis with enhanced expression of *SLC7A11*, a member of the cystine transporter xCT, and γ-glutamylcysteine synthetase to control ROS formation and tumor cell growth [46,50]. Thus, in addition to GDH and FH, OGC promotes tumor cell growth through regulation of oxidative stress by sustaining mGSH. Interestingly, OGC through the regulation of mGSH determines the susceptibility of cardiolipin to undergo oxidative modifications, which in turn regulates MOM-like LUVs permeabilization and MOMP [12]. Although cholesterol in mitochondria plays an anti-apoptotic role, in part by protecting MOM from Bax-induced permeabilization, the presence of CLOOH species antagonizes this function by facilitating the insertion of Bax into the bilayer without affecting its oligomerization. These findings are consistent with the current view pointing to MOM rather than BH3-only proteins as the only requirement for Bax/Bak activation and subsequent MOMP [51].

Given the role of OGC in mGSH regulation and HCC progression, we addressed potential mechanisms involved in the upregulation of OGC in HCC. Three different approaches leading to HIF-1α stabilization resulted in increased OGC expression, suggesting that OGC upregulation may be an additional mechanism whereby hypoxia/HIF-1α promotes tumorigenesis. Whether HIF-2α has an additional role in OGC regulation remains to be investigated. Furthermore, more work is required to understand why DIC is downregulated in HCC.

In summary, despite the fact that HCC exhibits mt-cholesterol accumulation, the overexpression of OGC overcomes the restriction in the transport of GSH into mitochondria and results in the paradoxical maintenance of mGSH pool. This event contributes to the reduced status of cardiolipin to ensure the inhibitory role of cholesterol in MOMP and cell death. Thus, OGC induction in HCC stands as a critical strategy to maintain adequate mGSH levels to control ROS generation, which along with mt-cholesterol loading, define an optimal scenario to withstand hypoxia tolerance and cell death by stabilizing mitochondrial membranes ensuring cell growth and tumor progression.

Grant support

The work was supported by grants SAF-2014-57674-R, SAF2015-66515-R and SAF-2015-69944-R from Plan Nacional de I+D, Spain and by the support of CIBEREHD; the center grant P50AA011999 Southern California Research Center for ALPD and Cirrhosis funded by NIAAA/

NIH; and support from AGAUR of the Generalitat de Catalunya 2014-SGR785, 2011BE-DGRBE100599 and 2011BEDGRBE100971 and grant LINK0378 from CSIC. The CSIC/UAB Proteomics Laboratory of IIBB-CSIC is a member of Proteored, PRB2-ISCIII and is supported by grant PT13/0001, of the PE I + D + i 2013–2016, funded by ISCIII and FEDER. We want to thank the Integrative Liver Cell Core (R24AA012885) for preparation of TICs.

Disclosure of potential conflict of interest

No potential conflict of interest was disclosed.

Acknowledgments

We want to acknowledge Dr. A. Colell for valuable suggestions and early support with mitochondrial cholesterol and GSH determinations and Dr. Milica Stefanovich for assistance with xenografts studies and Ester Sanchez-Jimenez for cardiolipin MS analyses. The technical assistance of Susana Nuñez is highly appreciated. We are indebted to Drs. Juan C. Garcia-Valdecasas and Josep Fuster for providing explants samples from patients with HCC.

Appendix A. Supporting information

Supplementary data associated with this article can be found in the online version at http://dx.doi.org/10.1016/j.redox.2017.08.022.

References

[1] Cancer Genome Atlas Research Network, J.N. Weinstein, E.A. Collisson, G.B. Mills, K.R. Shaw, B.A. Ozenberger, K. Ellrott, I. Shmulevich, C. Sander, J.M. Stuart, The cancer genome atlas pan-cancer analysis project, Nat. Genet. 45 (10) (2013) 1113–1120.
[2] R.C. Crain, R.W. Clark, B.E. Harvey, Role of lipid transfer proteins in the abnormal lipid content of Morris hepatoma mitochondria and microsomes, Cancer Res 43 (1983) 3197–3202.
[3] J. Montero, A. Morales, L. Llacuna, J.M. Lluis, O. Terrones, G. Basañez, et al., Mitochondrial cholesterol contributes to chemotherapy resistance in hepatocellular carcinoma, Cancer Res. 68 (2008) 5246–5256.
[4] B. Smith, H. Land, Anticancer activity of the cholesterol exporter ABCA1 gene, Cell Rep. 2 (2012) 580–590.
[5] E. Christenson, S. Merlin, M. Saito, P. Schlesinger, Cholesterol effects on BAX pore activation, J. Mol. Biol. 381 (5) (2008) 1168–1183.
[6] S. Lucken-Ardjomande, S. Montessuit, J.C. Martinou, Bax activation and stress-induced apoptosis delayed by the accumulation of cholesterol in mitochondrial membranes, Cell Death Differ. 15 (3) (2008) 484–493.
[7] S.D. Ha, S. Park, C.Y. Han, M.L. Nguyen, S.O. Kim, Cellular adaptation to anthrax lethal toxin-induced mitochondrial cholesterol enrichment, hyperpolarization, and reactive oxygen species generation through downregulating MLN64 in macrophages, Mol. Cell Biol. 32 (23) (2012) 4846–4860.
[8] M. Marí, F. Caballero, A. Colell, A. Morales, J. Caballeria, A. Fernandez, et al., Mitochondrial free cholesterol loading sensitizes to TNF- and Fas-mediated steatohepatitis, Cell Metab. 4 (3) (2006) 185–198.
[9] A. Fernández, L. Llacuna, J.C. Fernández-Checa, A. Colell, Mitochondrial cholesterol loading exacerbates amyloid beta peptide-induced inflammation and neurotoxicity, J. Neurosci. 29 (20) (2009) 6394–6405.
[10] A. Fernández, A. Colell, F. Caballero, N. Matías, C. García-Ruiz, J.C. Fernández-Checa, Mitochondrial S-adenosyl-L-methionine transport is insensitive to alcohol-mediated changes in membrane dynamics, Alcohol Clin. Exp. Res. 33 (7) (2009) 1169–1180.
[11] M. Bosch, M. Marí, A. Herms, A. Fernández, A. Fajardo, A. Kassan, et al., Caveolin-1 deficiency causes cholesterol-dependent mitochondrial dysfunction and apoptotic susceptibility, Curr. Biol. 2011 21 (8) (2011) 681–686.
[12] M. Marí, A. Colell, A. Morales, F. Caballero, A. Moles, A. Fernández, et al., Mechanism of mitochondrial glutathione-dependent hepatocellular susceptibility to TNF despite NF-kappaB activation, Gastroenterology 134 (5) (2008) 1507–1520.
[13] J. Mårtensson, J.C. Lai, A. Meister, High-affinity transport of glutathione is part of a multicomponent system essential for mitochondrial function, Proc. Natl. Acad. Sci. USA 87 (18) (1990) 7185–7189.
[14] S. Torres, N. Matías, A. Baulies, S. Nuñez, C. Alarcon-Vila, L. Martinez, et al., Mitochondrial GSH replenishment as a potential therapeutic approach for Niemann Pick type C disease, Redox Biol. 11 (2017) 60–72.
[15] C. von Montfort, N. Matias, A. Fernandez, R. Fucho, L. Conde de la Rosa, M.L. Martinez-Chantar, et al., Mitochondrial GSH determines the toxic or therapeutic potential of superoxide scavenging in steatohepatitis, J. Hepatol. 57 (2012) 852–859.
[16] L.H. Lash, D.A. Putt, L.H. Matherly, Protection of NRK-52E cells, a rat renal proximal tubular cell line, from chemical-induced apoptosis by overexpression of a mitochondrial glutathione transporter, J. Pharmacol. Exp. Ther. 303 (2) (2002) 476–486.
[17] L.H. Lash, Mitochondrial glutathione in diabetic nephropathy, J. Clin. Med. 4 (7) (2015) 1428–1447.
[18] H.M. Wilkins, S. Brock, J.J. Gray, D.A. Linseman, Stable over-expression of the 2-oxoglutarate carrier enhances neuronal cell resistance to oxidative stress via Bcl-2-dependent mitochondrial GSH transport, J. Neurochem. 130 (1) (2014) 75–86.
[19] C.K. Kamga, S.X. Zhang, Y. Wang, Dicarboxylate carrier-mediated glutathione transport is essential for reactive oxygen species homeostasis and normal respiration in rat brain mitochondria, Am. J. Physiol. Cell Physiol. 299 (2) (2010) C497–C505.
[20] O. Coll, A. Colell, C. García-Ruiz, N. Kaplowitz, J.C. Fernández-Checa, Sensitivity of the 2-oxoglutarate carrier to alcohol intake contributes to mitochondrial glutathione depletion, Hepatology 38 (3) (2003) 692–702.
[21] D. Han, R. Canali, D. Rettori, N. Kaplowitz, Effect of glutathione depletion on sites and topology of superoxide and hydrogen peroxide production in mitochondria, Mol. Pharmacol. 64 (5) (2003) 1136–1144.
[22] V. Ribas, C. García-Ruiz, J.C. Fernández-Checa, Glutathione and mitocondria, Front. Pharmacol. 5 (2014) 151.
[23] Z.T. Schug, E. Gottlieb, Cardiolipin acts as a mitochondrial signalling platform to launch apoptosis, Biochim Biophys. Acta 1788 (10) (2009) 2022–2031.
[24] V.E. Kagan, V.A. Tyurin, J. Jiang, Y.Y. Tyurina, V.B. Ritov, A.A. Amoscato, et al., Cytochrome c acts as a cardiolipin oxygenase required for release of proapoptotic factors, Nat. Chem. Biol. 1 (4) (2005) 223–232.
[25] J. Ji, A.E. Kline, A. Amoscato, A.K. Samhan-Arias, L.J. Sparvero, V.A. Tyurin, et al., Lipidomics identifies cardiolipin oxidation as a mitochondrial target for redox therapy of brain injury, Nat. Neurosci. 15 (10) (2012) 1407–1413.
[26] A. Colell, C. García-Ruiz, J.M. Lluis, O. Coll, M. Mari, J.C. Fernández-Checa, Cholesterol impairs the adenine nucleotide translocator-mediated mitochondrial permeability transition through altered membrane fluidity, J. Biol. Chem. 278 (36) (2003) 33928–33935.
[27] J.M. Lluis, A. Colell, C. García-Ruiz, N. Kaplowitz, J.C. Fernández-Checa, Acetaldehyde impairs mitochondrial glutathione transport in HepG2 cells through endoplasmic reticulum stress, Gastroenterology 124 (3) (2003) 708–724.
[28] N.S. Chandel, Mitochondrial regulation of oxygen sensing, Avd. Exp. Med. Biol. 661 (2010) 339–354.
[29] R.B. Hamanaka, S.E. Weinberg, C.R. Reczek, N.S. Chandel, The mitochondrial respiratory chain is required for organismal adaptation to hypoxia, Cell Rep. 15 (3) (2016) 451–459.
[30] S.S. Sabharwal, P.T. Schumacker, Mitochondrial ROS in cancer: initiators, amplifiers or an Achilles' heel? Nat. Rev. Cancer 14 (11) (2014) 709–721.
[31] G.B. Waypa, K.A. Smith, P.T. Schumacker, O2 sensing, mitochondria and ROS signaling: the fog is lifting, Mol. Asp. Med. 47–48 (2016) 76–89.
[32] M.M. Alam, S. Lal, K.E. FitzGerald, L. Zhang, A holistic view of cancer bioenergetics: mitochondrial function and respiration play fundamental roles in the development and progression of diverse tumors, Clin. Transl. Med. 5 (1) (2016) 3.
[33] A. Viale, P. Pettazzoni, C.A. Lyssiotis, H. Ying, N. Sánchez, M. Marchesini, et al., Oncogene ablation-resistant pancreatic cancer cells depend on mitochondrial function, Nature 514 (7524) (2014) 628–632.
[34] C. Garcia-Ruiz, A. Colell, A. Morales, N. Kaplowitz, J.C. Fernández-Checa, Role of oxidative stress generated from the mitochondrial electron transport chain and mitochondrial glutathione status in loss of mitochondrial function and activation of transcription factor nuclear factor-kappa B: studies with isolated mitochondria and rat hepatocytes, Mol. Pharmacol. 48 (5) (1995) 825–834.
[35] G. Chen, Z. Chen, Y. Hu, P. Huang, Inhibition of mitochondrial respiration and rapid depletion of mitochondrial glutathione by beta-phenethyl isothiocyanate: mechanisms for anti-leukemia activity, Antioxid. Redox Signal. 15 (2011) 2911–2921.
[36] D. Anastasiou, G. Poulogiannis, J.M. Asara, M.B. Boxer, J.K. Jiang, M. Shen, et al., Inhibition of pyruvate kinase M2 by reactive oxygen species contributes to cellular antioxidant responses, Science 334 (2011) 1278–1283.
[37] C.M. Grant, K.A. Quinn, I.W. Dawes, Differential protein S-thiolation of glyceraldehyde-3-phosphate dehydrogenase isoenzymes influences sensitivity to oxidative stress, Mol. Cell Biol. 19 (1999) 2650–2656.
[38] M. Gallo, D. Park, D.S. Luciani, K. Kida, F. Palmieri, O.E. Blacque, et al., MISC-1/OGC links mitochondrial metabolism, apoptosis and insulin secretion, PloS One 6 (3) (2011) e17827.
[39] A. Masini, D. Ceccarelli, D. Gallesi, F. Giovannini, T. Trenti, Lipid hydroperoxide induced mitochondrial dysfunction following acute ethanol intoxication in rats. The critical role for mitochondrial reduced glutathione, Biochem. Pharmacol. 47 (1994) 217–224.
[40] C.L. Chen, H. Tsukamoto, J.C. Liu, C. Kashiwabara, D. Feldman, L. Sher, et al., Reciprocal regulation by TLR4 and TGF-β in tumor-initiating stem-like cells, J. Clin. Investig. 123 (7) (2013) 2832–2849.
[41] P. Gao, H. Zhang, R. Dinavahi, F. Li, Y. Xiang, V. Raman, et al., HIF-dependent antitumorigenic effect of antioxidants in vivo, Cancer Cell 12 (3) (2007) 230–238.
[42] K. Irani, Y. Xia, J.L. Zweier, S.J. Sollott, C.J. Der, E.R. Fearon, M, et al., Mitogenic signaling mediated by oxidants in Ras-transformed fibroblasts, Science 275 (1997) 1649–1652.
[43] V.I. Sayin, M.X. Ibrahim, E. Larsson, J.A. Nilsson, P. Lindahl, M.O. Bergo, Antioxidants accelerate lung cancer progression in mice, Sci. Transl. Med. 6 (221) (2014) 221ra15.
[44] K. Le Gal, M.X. Ibrahim, C. Wiel, V.I. Sayin, M.K. Akula, C. Karlsson, et al., Antioxidants can increase melanoma metastasis in mice, Sci. Transl. Med. 7 (308) (2015) 308re8.
[45] L. Raj, T. Ide, A.U. Gurkar, M. Foley, M. Schenone, X. Li, N.J. Tolliday, et al.,

Selective killing of cancer cells by a small molecule targeting the stress response to ROS, Nature 475 (7355) (2011) 231–234.
[46] L. Zheng, S. Cardaci, L. Jerby, E.D. MacKenzie, M. Sciacovelli, T.I. Johnson, et al., Fumarate induces redox-dependent senescence by modifying glutathione metabolism, Nat. Commun. 6 (2015) 6001.
[47] Z. Chen, D.A. Putt, L.H. Lash, Enrichment and functional reconstitution of glutathione transport activity from rabbit kidney mitochondrial: further evidence for the role of the dicarboxylate and 2-oxoglutarate cirriers in mitochondrial glutathione transport, Arch. Biochem. Biophys. 373 (2000) 193–202.
[48] L.M. Booty, M.S. King, C. Thangaratnarajah, H. Majd, A.M. James, E.R. Kunji, M.P. Murphy, The mitochondrial dicarboxylate and 2-oxoglutarate carriers do not transport glutathione, FEBS Lett. 589 (5) (2015) 621–628.
[49] L. Jin, D. Li, G.N. Alesi, J. Fan, H.B. Kang, Z. Lu, et al., Glutamate dehydrogenase 1 signals through antioxidant glutathione peroxidase 1 to regulate redox homeostasis and tumor growth, Cancer Cell 27 (2) (2015) 257–270.
[50] L.B. Sullivan, E. Martinez-Garcia, H. Nguyen, A.R. Mullen, E. Dufour, S. Sudarshan, et al., The proto-oncometabolite fumarate binds glutathione to amplify ROS-dependent signaling, Mol. Cell 51 (2) (2013) 236–248.
[51] K.L. O´Neill, K. Huang, J. Zhang, Y. Chen, X. Luo, Inactivation of prosurvival Bcl-2 proteins activates Bax/Bak through the outer mitochondrial membrane, Genes Dev. 30 (2016) 973–988.